CrossMark

Biological evaluation of ultra-fine titanium with improved mechanical strength for dental implant engineering

Lucie Ostrovska[1] · Lucie Vistejnova[1] · Jan Dzugan[2] · Peter Slama[2] ·
Tomas Kubina[2] · Egor Ukraintsev[3] · Dana Kubies[4] · Milena Kralickova[1] ·
Marie Hubalek Kalbacova[1,5]

Abstract Titanium, the gold standard for dental implant materials, is distinguished by its exceptional biocompatibility; however, from a long-term perspective, titanium still lacks sufficient loading strength. Commercially pure titanium with grain size 30 μm was processed by equal channel angular pressing, and two novel mechanically improved types of titanium material with grain size 4.6 and ≤ 1 μm were obtained. The surfaces of these ultra-fine grained titanium samples were further mechanically treated by grinding and polishing, and their surfaces were characterized by atomic force microscopy and contact angle measurement. Osteoblast-like cells and human mesenchymal stem cells were used to evaluate the cytocompatibility of these titanium samples. The cell metabolic activity, cell number, cell area, morphology, and cell adhesion quality during the early stage (2 h) and prolonged cultivation (48 h) were determined. Both cell types displayed increased initial attachment to all tested titanium materials in comparison to reference tissue culture plastic. Importantly, results revealed that the novel titanium materials with improved strength were equivalent to the original commercially pure titanium, thus confirming their suitability for osteoblast and mesenchymal stem cell growth and proliferation. The present study proved the cytocompatibility of the novel forms of titanium with superior mechanical properties and revealed their potential for manufacturing of long-term dental implants.

Introduction

Modern dentistry represents well-established field of medicine dealing with the increasing patient demands on implant function, permanence, and esthetics. Due to technological and medical progress, biocompatible materials with excellent mechanical properties have been

✉ Marie Hubalek Kalbacova
marie.kalbacova@lf1.cuni.cz

Lucie Ostrovska
Lucie.Ostrovska@lfp.cuni.cz

Lucie Vistejnova
Lucie.Vistejnova@lfp.cuni.cz

Jan Dzugan
jan.dzugan@comtesfht.cz

Peter Slama
peter.slama@comtesfht.cz

Tomas Kubina
tomas.kubina@comtesfht.cz

Egor Ukraintsev
ukraints@fzu.cz

Dana Kubies
kubies@imc.cas.cz

Milena Kralickova
Milena.Kralickova@lfp.cuni.cz

[1] Biomedical Center, Faculty of Medicine in Pilsen, Charles University in Prague, Alej Svobody 76, 323 00 Pilsen, Czech Republic

[2] COMTES FHT a.s., Prumyslova 995, 334 41 Dobrany, Czech Republic

[3] Institute of Physics, Academy of Sciences of the Czech Republic, Na Slovance 1999/2, 182 21 Prague, Czech Republic

[4] Institute of Macromolecular Chemistry, Academy of Sciences of the Czech Republic, Heyrovskeho namesti 2, 162 06 Prague, Czech Republic

[5] Institute of Inherited Metabolic Disorders, 1st Faculty of Medicine, Charles University in Prague, Ke Karlovu 2, 128 08 Prague, Czech Republic

successfully designed; however, ensuring their longevity, particularly under load-bearing conditions, remains difficult [1–3].

Titanium (Ti) is one of the best materials for the production of dental and orthopedic implants. Many metallic materials are not suitable for applications in living organisms due to their high reactivity and inflammatory process activation; therefore, currently, only suitable metallic alloys are being used [4, 5]. Ti is distinguished by its biocompatibility, low reactivity in tissue, and corrosion resistance, which is provided by a passive layer of TiO_2 that forms spontaneously on the surface. This layer represents an inert barrier between the material and the biological environment, which in clinical practice means that the implant is prevented from releasing ions into the organism [6]. Moreover, Ti is characterized by its light weight and high formability, which enables the easy fabrication of different low-weight medical devices [7]. The low elastic modulus of Ti is advantageous over other metals because it decreases the shield stress of the implant, which is particularly important in bone tissue. Nevertheless, the primary issue of the insufficient loading strength of Ti remains [8]. A significant improvement of this characteristic was achieved by fabricating a duplex alloy with aluminum and vanadium, which resulted in the formation of the most successful and widely used Ti alloy, Ti-6Al-4 V. Originally, this alloy was designed for utilization in aerospace engineering, and its suitable properties for use in biomedicine were discovered as an afterthought [9]. Unfortunately, from a long-term perspective, the utilization of Ti-6Al-4V increases the risk of the passive dissolution of metal ions into the surrounding tissue because the layer of TiO_2 loses its barrier function in alloys after recurrent wear and fretting. Slow and gradual ion release is dangerous because this process can lead to the accumulation of toxic amounts of aluminum and vanadium in an organism, thus posing a risk of severe systemic tissue damage. Therefore, Ti-alloys with toxic elements are not used for the replacement of movable joints where sliding contact occurs [6, 10].

Currently, new approaches to improve the mechanical characteristics of Ti include the following: (a) replacing the potentially toxic elements in the alloys with non-toxic elements, and (b) grain refinement [11]. New alloys composed of tantalum (Ta), nickel (Ni), zirconium (Zr), molybdenum (Mo), or niobium (Nb) have been already generally in use [12], although their manufacturing sometimes requires high costs (Mo, Ta). However, the sensitivity of the population to previously non-toxic elements increases (for example, Ni) when these alloys are used [13]. In contrast, strengthening commercially pure Ti (cp Ti) by refining the grain size to the nanoscale can extend its long-term performance and improve the mechanical strength of an implant, while preserving its exceptional biocompatibility due to eliminated release of toxic ions. Specific criteria must be met when developing methods for nanostructuring Ti for further biomedical utilization. Selected production techniques must guarantee the manufacture of uniformly defined microstructures within the bulk material that are stable after further processing. A widely used technology for metal nanostructuring is severe plastic deformation (SPD), which forms ultra-fine grain (UFG) materials from a bulk coarse-grained material using extremely high strain [14]. One of the most developed techniques of SPD is equal channel angular pressing (ECAP), which works on the principle of a simple shear force applied on a rod-shaped billet [15]. Thermal stability of Ti-Alloys processed by SPD techniques, such as ECAP, is up to 450 °C as referred in [16, 17]. Additionally, surface of the materials should mimic the three-dimensional extracellular environment of bone tissue and thus stimulate cell attachment and proliferation. Specific surfaces of bio-implants with micro/nano-topographies can greatly enhance the adhesion of cells, particularly in mesenchymal stem cells and osteoblasts [18–20]. Such treatment can be performed by many techniques, including acid etching, plasma blasting, sand/grit blasting or mechanical polishing and grinding [21]. Enhanced cell adhesion to the surface is crucial for better acceptance of the implant by an organism, and proper long-term cell contact with the material can avoid the creation of deep pockets on the interface, which can lead to bacterial infection [22].

The aim of our study was to evaluate the cytocompatibility of cp Ti Grade 2 processed by ECAP-Conform using the human osteoblast-like cell line SAOS-2 and human mesenchymal stem cells (hMSCs). Six types of Ti with different grain sizes and different mechanical surface treatments were tested. The interactions and viability of the cells with the materials were investigated during the early stages of attachment after short (2 h) and long (48 h) periods.

Materials and methods

Sample fabrication and mechanical characterization

Ti samples were supplied by COMTES FHT a.s. (Dobrany, Czech Republic) in the form of discs with diameters of 8 mm (~ 0.5 cm^2). The Grade 2 cp Ti (S) was used as a substrate for subsequent processing by ECAP-Conform [15]. The chemical purity and composition of the bulk Ti material were measured using a Q4 Tasman optical emission spectrometer (Bruker, USA) and a G8 Galileo gas analyzer (Bruker, USA). The original material (S) was passed once (M) or three times (Z) through ECAP-

Conform, and three different Ti samples with the following grain sizes were obtained: Z (≤ 1 μm), M (4.6 μm), and S (30 μm). The microstructure of Z and M materials was confirmed by electron backscatter diffraction (EBSD) maps acquired in SEM JEOL 7400F (JEOL Ltd., Japan) by EBSD camera Oxford Nordlys (Oxford Instruments, United Kingdom). Very fine grains of the material Z were investigated by TEM JEOL 200CX (JEOL Ltd., Japan). Quasi-static tensile tests were performed according to ISO 6892-1 on triplicates of the investigated Ti samples at room temperature. Round tensile specimens with threaded shoulders of diameter 4 mm and with gauge lengths of 20 mm were tested. Tests were performed using a Zwick Z 250 electro-mechanical testing system (Zwick Roell, Germany) fitted with hydraulic grips. The strain on the sample was measured directly using a Messphysik laser speckle extensometer (Messphysik materials testing, Austria), which allows for biaxial strain measurement until the specimen fractures. The specimens' dimensions were measured using a micrometer before testing, and their gauge lengths were marked for elongation evaluation. The appropriate dimensions were measured after the tests to evaluate elongation and cross-section reduction. The elongation shown in Fig. 1 is evaluated from marks on the specimen. The surface of each Ti sample was treated by polishing with diamond paste and colloidal silica (p) or by grinding with abrasive grinding paper (1200) (g). Thus, six types of Ti samples were evaluated, i.e., Zp, Zg, Mp, and Mg, representing the new titanium materials with improved mechanical properties, and Sp and Sg, representing the original Ti material. All Ti samples were compared with common polystyrene material for cell cultivation (PS control).

Surface topography characterization

Qualitative and quantitative analyses of the surface morphology of the Ti samples and PS control were performed using atomic force microscopy (AFM). A Ti sample area of 50×50 μm was studied in air using a Peakforce AFM system (ICON, Bruker, USA) in quantitative nanomechanical mapping mode with a Multi75Al cantilever (BudgetSensors, Innovative Solutions Bulgaria Ltd, Bulgaria). In this mode, the interaction between the tip and the sample is controlled and measured at each point. The cantilever was treated using CF_4 plasma to reduce the contamination and interaction with the surfaces of the Ti samples. The primary advantage of this mode is its ability to measure using small forces; moreover, measuring the elastic modulus of the material and the adhesion between the AFM tip and the sample is possible using this mode [23]. Two samples of each type of surface were scanned, their topographic features were examined, and the root mean square roughness (R_{RMS}) of each Ti sample was quantitatively estimated.
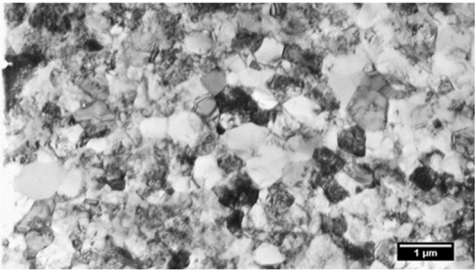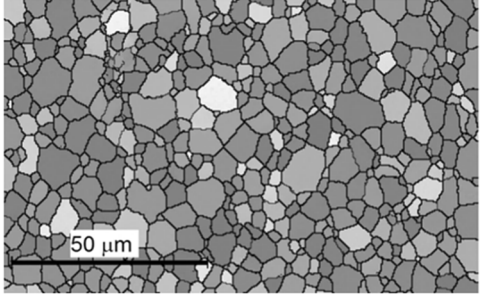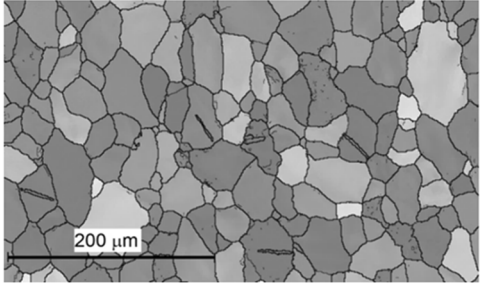
Wettability measurement

The surface wettability of the Ti samples and of the PS control was examined with a static and dynamic sessile water drop method using an OCA 20 contact angle apparatus (DataPhysics, Germany). Before the analysis, the Ti samples were cleaned by gentle rinsing in petroleum ether, methanol, and then water to remove impurities due to sample processing [24]. Then, the samples were sterilized in 70 % ethanol for 10 min and rinsed two times with deionized water to simulate the conditions of in vitro experiments. Finally, the Ti samples were dried under a stream of nitrogen in a flow box and subjected to analysis. For the static method analysis, each sample was characterized using two drops with volumes of 2 μl. The data were evaluated using the Young–Laplace method. For the dynamic method analysis, a 3 μl drop was placed on the surface, and advancing and receding contact angles were determined, while the volume of the drop was increased to 8 μl and decreased at a flow rate of 0.2 μl/s. The data were evaluated using the tangent leaning method. Three Ti samples of each surface type were measured twice by the static method and once by the dynamic method.

Cell culture

The SAOS-2 cells (DSMZ, Germany) were cultured in McCoy's 5A medium without phenol red (HyClone, USA) supplemented with heat-inactivated 15 % fetal bovine serum (GE Healthcare, UK), 10,000 U/ml penicillin (Sigma-Aldrich, USA), and 10 μg/ml streptomycin (Sigma-Aldrich, USA). The cells were seeded at a density of 15,000 cells/cm^2.

The hMSCs (General University Hospital, Prague and University Hospital, Pilsen) were obtained from four patients undergoing diagnostic trephine biopsies for suspected hematological disease without tumor-affected bone marrow and from volunteers after giving written consent. This research conforms to general ethical principles and standards—all the procedures involving living human participants were approved by the Ethical Committee of General University Hospital in Prague and by University Hospital and Medical Faculty in Pilsen, Charles University in Prague. The isolated cells were cultured in alpha minimum essential medium (α-MEM; Gibco, USA) supplemented with heat-inactivated 10 % fetal bovine serum (GE Healthcare, UK), 10,000 U/ml penicillin (Sigma-Aldrich, USA), and 10 μg/ml streptomycin (Sigma-Aldrich, USA). The hMSCs were seeded at a density of 10,000 cells/cm^2 and cultured up to the 5th passage.

Fig. 1 Summary of strength and plastic characteristics of Ti samples including representative microstructural images of Ti samples showing grain size of materials. **a** Transmission electron microscope (TEM) image; **b** and **c** electron backscatter diffraction (EBSD) maps

(a)		
Grain size (μm)	≤ 1.0	
Yield stress (MPa)	575.8 ± 8.8	
Tensile strength (MPa)	656.8 ± 6.3	Z
Elongation (%)	22.4 ± 5.1	
Cross section reduction (%)	60.4 ± 0.7	
(b)		
Grain size (μm)	4.6	
Yield stress (MPa)	409.9 ± 7.7	
Tensile strength (MPa)	516.2 ± 1.8	M
Elongation (%)	30.9 ± 1.7	
Cross section reduction (%)	59.6 ± 1.5	
(c)		
Grain size (μm)	30.0	
Yield stress (MPa)	332.6 ± 1.8	
Tensile strength (MPa)	468.2 ± 1.9	S
Elongation (%)	31.4 ± 1.4	
Cross section reduction (%)	62.9 ± 0.5	

Ti samples were placed on the bottom of 24-well plates (Techno Plastic Products, Switzerland) in doublets. The sterilization process was performed before cultivation. The samples were rinsed with 70 % ethanol for 10 min and then washed twice with deionized water.

Each cell type was plated onto the Ti samples at the density listed above using the droplet technique. Briefly, 100 μl of cell suspension was dropped onto Ti samples, and 380 μl of the cell suspension was dropped onto PS control wells to obtain identical cell densities on the surface. The cells were cultured for 2 or 48 h in a humidified 5 % CO_2 atmosphere at 37 °C. To prevent droplet evaporation, the Ti samples and PS control were covered with additional complete culture media to a volume of 1000 μl at 1 h after initial attachment, and the cells were further cultured until the desired time points.

Metabolic activity

The metabolic activity of the cells at 48 h after plating was assessed by MTS assay (Cell Titer96® AqueousOne,

Promega, USA). The principle of this colorimetric assay is the reduction of the MTS ((3-(4,5-dimethylthiazol-2-yl)-5-(3-carboxymethoxyphenyl)-2-(4-sulfophenyl)-2H-tetrazolium)) compound into a soluble colored formazan product by mitochondrial dehydrogenases. The assay was performed according to the manufacturer's protocol. After the cells were incubated for 2 h with MTS reagent, the optical density was measured using a microplate reader (Infinite® 200 PRO, Tecan Group Ltd., Switzerland) at 490 nm, subtracting the background at 655 nm. The obtained results were compared to the results of the cells on the PS control. These results are expressed as percentages.

Fluorescence microscopy

After 2 and 48 h, the cells were fixed in 4 % paraformaldehyde. Then, the nuclei were stained with DAPI (1:1000, Sigma-Aldrich, USA), actin filaments were stained with Phalloidin-Alexa Fluor 488 (1:1000, Invitrogen, USA), and the vinculin protein in cell focal adhesions was visualized by antibodies (mouse monoclonal anti-

vinculin antibody, 1:500, Sigma-Aldrich, USA and Alexa Fluor 568-conjugated goat anti-mouse antibody, 1:500, Invitrogen, USA). An Eclipse Ti-S or Eclipse Ti-U epifluorescence microscope (Nikon, Japan) and a DS-Qi1Mc digital camera (Nikon, Japan) were used to acquire fluorescence images of the stained cells.

Cell number and cell area

For cell number determination, ten random fluorescence images of DAPI-stained nuclei from every Ti sample and PS control were acquired using a fluorescence microscope at $10\times$ magnification. For cell area determination, ten random fluorescence images of DAPI-stained nuclei and phalloidin-Alexa488-stained actin filaments were acquired for every Ti sample and PS control using a fluorescence microscope at $20 \times$ magnification. The cell nuclei were automatically counted, and the single cell area was estimated using ImageJ [25] and Cell Profiler [26]. The cell number is expressed as the number of cells per cm^2. The cell area is expressed as the mean area of the cell in μm^2 for every substrate. The results obtained from both analyses were compared to the results of cells on the PS control. These results are expressed as percentages.

Statistical analysis

All presented data were derived from at least two independent experiments performed in duplicate. The results are presented as the mean values with error bars indicating standard deviations. Data distribution was evaluated using the Shapiro–Wilk test. The non-parametric Wilcoxon matched-pairs test was used to determine significant differences between the datasets from the Ti samples and the PS control. An ANOVA was used to compare Ti samples to each other. P values of less than 0.05 were considered statistically significant. Statistical analysis was performed using the software STATISTICA (StatSoft, Inc., USA).

Results

Chemical and mechanical characterization of Ti samples

The chemical purity and composition of the original Ti material (S) were examined before undergoing the ECAP-Conform process. The listed weight percentages of the elements (Table 1) show that the bulk material was composed of 99.80 % Ti. The mechanical characterization of each of the three Ti samples without surface treatment involved determining their strength characteristics (yield stress and tensile strength) and plastic characteristics (elongation and cross-section reduction). The measured values and representative microstructure images are summarized in Fig. 1, and the resultant stress–strain curves for each Ti sample are shown in Fig. 2. The original S samples exhibited the lowest strength parameters and had the grains with the largest area. The M samples exhibited slight increases in their mechanical properties of approximately 15 %, while maintaining almost the same deformation behavior as the S samples. The highest stress–strain curves were obtained in the case of the Z samples, as they exceeded the S samples by more than 30 % while maintaining sufficient ductility for potential further product formation. The Z samples exhibited superior properties to the other investigated samples.

Surface topography of Ti samples

Characterization of the surface topography of all Ti samples and the PS control was performed by AFM. The surface profiles are presented in diagrams in Fig. 3. Quantitative measurements of the R_{RMS} were also conducted for each material (Table 2). The obtained AFM data show that the polished samples have a fine topography and lack distinctive surface roughness and tall peaks. The Zp samples revealed many small 10 nm deep holes and occasional large-scale roughness (~ 5 μm in X–Y directions). On the Mp samples, many 10–20 nm tall Ti particles above a flat layer were detectable. Sp samples were of a similar topography as Mp samples, with fewer tall particles, which was most likely caused by the larger grain size of the S samples.

In contrast, all ground samples had an RMS roughness of approximately 270 nm, irrespective of the grain size. The width of the 500–1000 nm tall peaks was 10 ± 3 μm for all Ti samples. Even on a smaller scale (10 μm), the morphologies of Zg, Mg, and Sg samples were similar (data not shown). Furthermore, AFM data showed that tall objects, holes, and flat regions of all Ti samples had similar elastic moduli (data not shown), confirming that the tall objects on the surface are of Ti origin.

Surface wettability of Ti samples

The wettability of Ti samples and the PS control was determined by water contact angle (θ) measurements using static and dynamic (advanced and receding θ) sessile drop methods. The results are presented in Table 2. The tested

Table 1 Chemical composition of Ti bulk material (wt%)

Fe	O	C	H	N	Ti
0.0460	0.1200	0.0230	0.0026	0.0074	99.8010

Fig. 2 Mechanical characteristics of Ti samples. Stress–strain curves of Ti samples (triplets)
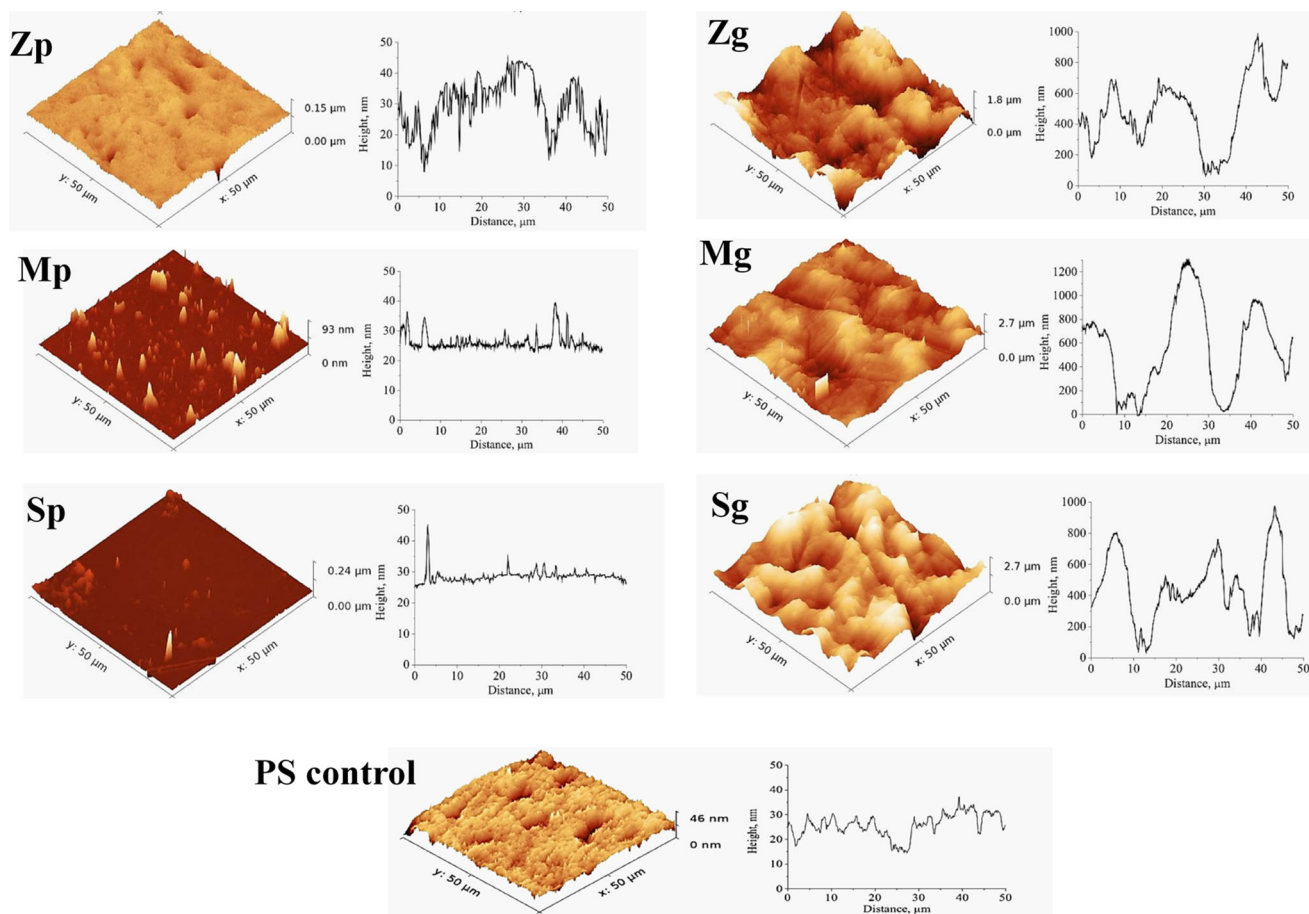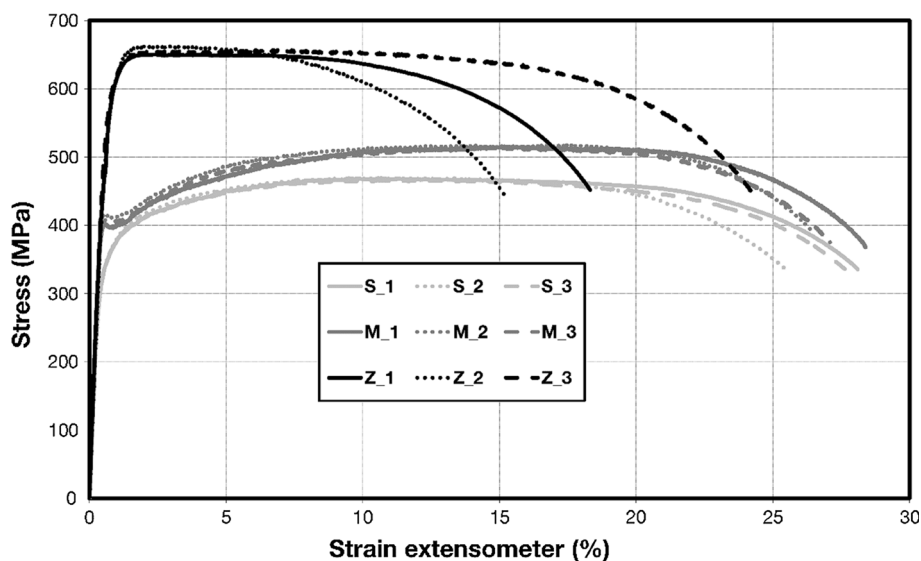

Fig. 3 AFM images of Ti samples and polystyrene (PS) control with corresponding 2D diagrams of height profiles

Ti samples represented hydrophilic surfaces with a static θ between 30° and 45° based on the surface treatment. θ values obtained by the static measurement method were generally 5° lower than the values of the advanced θ (θ_A)

obtained by the dynamic method. However, the trend between Ti samples remained similar. Importantly, the receding θ (θ_R) was not determined by the dynamic method in the case of all Ti samples, indicating profound water

Table 2 Quantitative characterization of the surface of Ti samples and polystyrene (PS) control

Surface	Grain size (μm)	Surface treatment	R_{RMS} (nm)	Static contact angle θ (°)	Dynamic contact angle	
					θ_A (°)	θ_R (°)
PS control	–	–	4.7	69.0 ± 1.4	71.0 ± 1.1	22.7 ± 0.5
Zp	≤1.0	Polished	2.0–5.0	44.0 ± 1.3	49.0 ± 0.5	N/A
Mp	4.6	Polished	2.0–5.0	43.0 ± 1.3	47.0 ± 1.8	N/A
Sp	30.0	Polished	5.0–12.0	41.0 ± 0.8	46.0 ± 0.1	N/A
Zg	≤1.0	Ground	∼270.0	34.0 ± 0.5	37.0 ± 0.6	N/A
Mg	4.6	Ground	∼270.0	30.0 ± 1.0	35.0 ± 0.0	N/A
Sg	30.0	Ground	∼270.0	34.0 ± 0.3	41.0 ± 0.9	N/A

R_{RMS} root mean squared roughness, θ_A advancing contact angle, θ_R receding contact angle

interactions with Ti samples that could not be evaluated using only the static θ analysis. Water was adsorbed and retained on all Ti samples more strongly than on the PS control, with θ_R of 22°.

The surfaces of the polished samples (Zp, Mp, Sp) showed dynamic θ_A values between 46° and 49°. A slight tendency of θ_A to decrease with increasing grain size was also observed. The θ_A values obtained for the ground samples (Zg, Mg, Sg) were approximately 10° lower than the values of the polished samples. Here, the grain sizes of the material did not affect the surface wettability. Thus, treatment by grinding resulted in more hydrophilic surfaces.

Cell metabolic activity on Ti samples

The metabolic activity of the cells on the Ti samples was assessed after 48 h of incubation. For SAOS-2 cells, no significant difference was observed between the Ti samples and the PS control (Fig. 4a). Moreover, no obvious difference was observed even among the different Ti samples. The slightly decreased metabolic activity of the cells plated on both *M* samples compared to the cells plated on PS control was not statistically significant. In the case of hMSCs (Fig. 4b), the metabolic activity did not differ significantly between the cells cultivated on Ti samples and on the PS control, except for ground *M* and *S* samples, where the slight decrease was statistically significant.

Cell number

The number of cells on the Ti samples was measured after 2 and 48 h of cultivation to assess the extent of the initial attachment of the cells to the material and to define their growth during cultivation (Fig. 5).

The number of adherent SAOS-2 cells on Ti samples during the first 2 h was substantially higher than the number of these cells on the PS control (Fig. 5a). This considerable increase in the number of adherent SAOS-2 cells at this initial phase was comparable among all Ti samples. The difference between the Ti samples and the PS control remained significant even after 48 h of incubation. However, the increase in the cell numbers on the Ti samples in comparison to the PS control was more pronounced after 2 h (3-fold) than after 48 h (2-fold) of incubation (Fig. 5c), suggesting a slower growth of SAOS-2 cells on Ti samples.

hMSCs also showed higher numbers of adherent cells on the Ti samples compared to the PS control after a 2-h incubation (Fig. 5b); however, the increases were not significant in all cases. In contrast, after 48 h, the cell number on the PS control was higher compared to all Ti samples. Similar to SAOS-2, the increase in the cell number on the Ti samples was slower than on the PS control. However, in the case of hMSCs, the difference was even more pronounced (Fig. 5d), which led to the lowered cell number on the Ti samples after 48 h in comparison to the PS control.

Cell area

The areas of single cells were determined after 2 and 48 h of cultivation. The determination of both cell type areas indicated very similar features for both time points of the assessment (Fig. 6). The real cell area on the PS samples is presented in Fig. 6a. From the beginning, both cell types plated on the Ti samples were smaller than those plated on the PS control. After 2 h of incubation, the area of SAOS-2 cells cultivated on the Ti samples was only fractionally smaller than that on the PS control (Fig. 6b), with significant differences found only for Zp, Mp, and Sg. In contrast, hMSCs were significantly smaller on most of the Ti samples compared to those cultivated on the PS control (approximately, a 20 % size reduction) (Fig. 6c).

The area differences were more pronounced after 48 h of cultivation. The areas of SAOS-2 cells were reduced by approximately 20 %; however, the areas of hMSCs on all Ti samples were reduced even more (by approximately 50 % in comparison to the PS control).
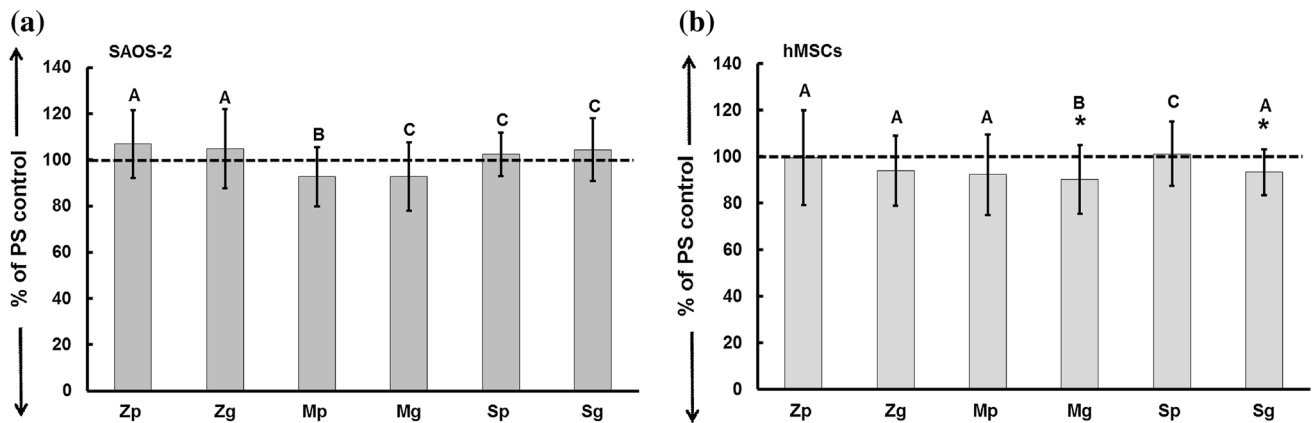
(a)

(b)

Fig. 4 Metabolic activity after 48 h of cultivation on Ti samples. **a** Osteoblasts (SAOS-2), **b** human mesenchymal stem cells (hMSC). Relative values are expressed as a percentage of PS control (*dashed line*). Asterisk (*) means a significant difference from PS control

(Wilcoxon matched-pairs test, $p < 0.05$). Groups marked with *different letters* express significant inter-group difference within samples (ANOVA, LSD post hoc test, $p < 0.05$)
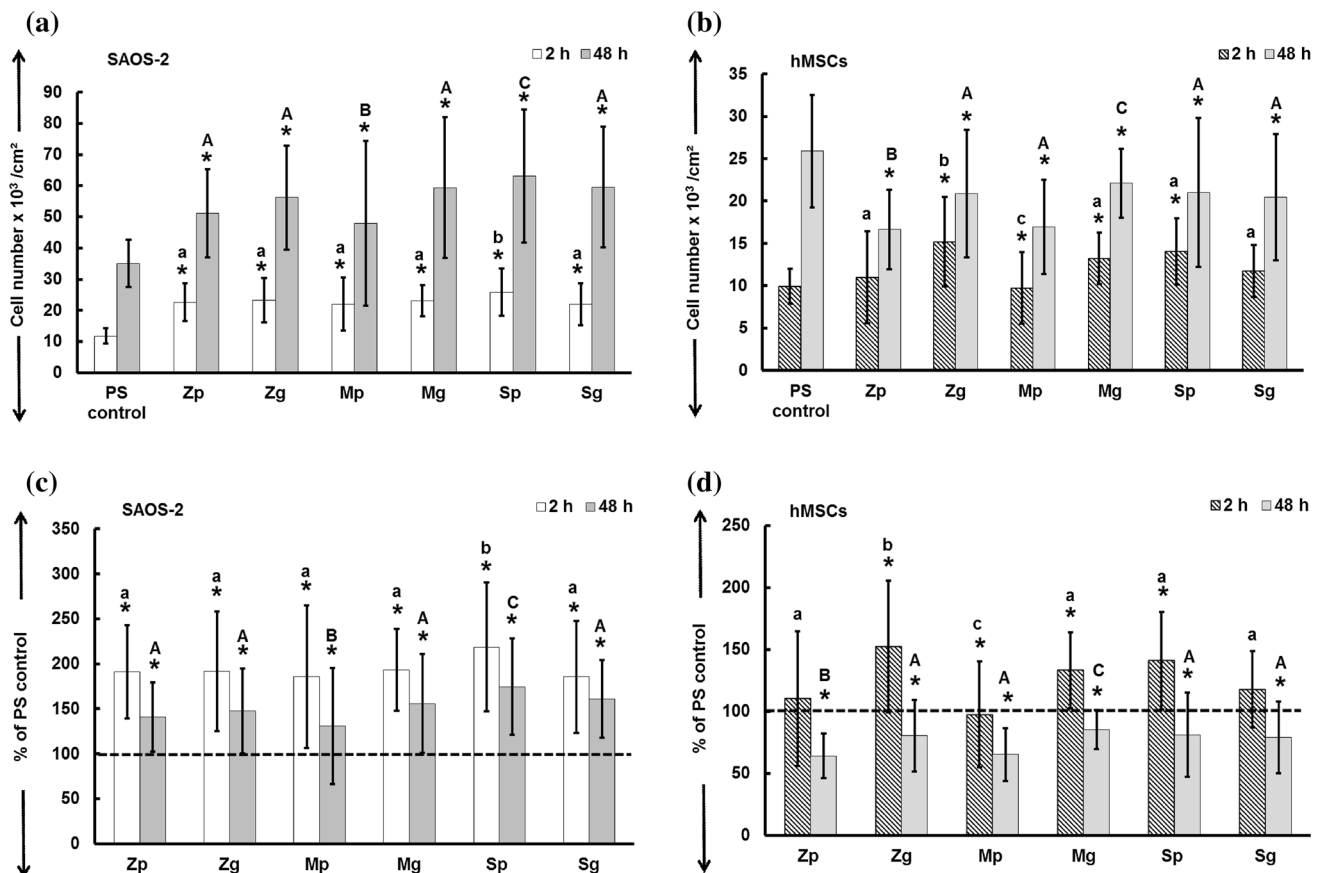
(a)

(b)

(c)

(d)

Fig. 5 Cell number after 2 and 48 h of cultivation on Ti samples. **a** Osteoblasts (SAOS-2)—values of cell number/cm², **b** human mesenchymal stem cells (hMSCs)—values of cell number/cm², **c** osteoblasts (SAOS-2)—relative values expressed as a percentage of PS control (*dashed line*), **d** human mesenchymal stem cells (hMSCs)—relative values expressed as a percentage of PS control

(*dashed line*). Asterisk (*) means a significant difference from PS control (Wilcoxon matched-pairs test, $p < 0.05$). Groups marked with *different lower-case letters* (2 h) or with different *upper-case letters* (48 h) express significant inter-group difference within samples (ANOVA, LSD post hoc test, $p < 0.05$)

Cell morphology and adhesion

The cell morphology on different Ti samples was analyzed by the double fluorescence staining of actin filaments and nuclei after 48 h (Fig. 7). Moreover, vinculin, as an intracellular protein participating in the formation of focal adhesions, was also visualized by immunofluorescence staining to investigate the quality of focal adhesion plaques of SAOS-2 cells on different Ti samples (Fig. 8). Representative images of cells cultivated on the different substrates are shown in Fig. 7. A common cuboidal-like morphology was displayed by SAOS-2 cells on all Ti samples (Fig. 7b, c) as well as on the PS control (Fig. 7a). Thus, in spite of the observed smaller sizes of these cells on Ti samples, their morphology and cytoskeleton quality were comparable to those cultivated on the PS control and were not altered. The morphology of hMSCs grown on Ti samples (Fig. 7e, f) and on the PS control (Fig. 7d) differed. hMSCs cultured on ground samples displayed noticeable elongation and filopodia extensions, and their spreading to the orientation of valley-like structures was

more intense. Polished samples enabled the growth and spreading of hMSCs in all directions; thus, their morphology varied, and they often grew in vertical layers.

The most pronounced focal adhesions were observed in SAOS-2 cells, as shown in Fig. 8. In particular, the cells cultured on ground samples displayed noticeable focal adhesion plaques (Fig. 8e–g), where the most of the vinculin signal was localized in the form of circular structures on the edges and extensions of the cells. By contrast, SAOS-2 cells grown on polished samples exhibited elongated focal adhesions localized on the entire basal pole of the cells and displayed strong similarity with the cells cultured on the PS control (Fig. 8b–d).

Discussion

The biocompatibility of the material is not the only parameter that defines the lifespan of an implant. Long-term stress conditions demand a material that represents an excellent combination of strength and plastic properties.
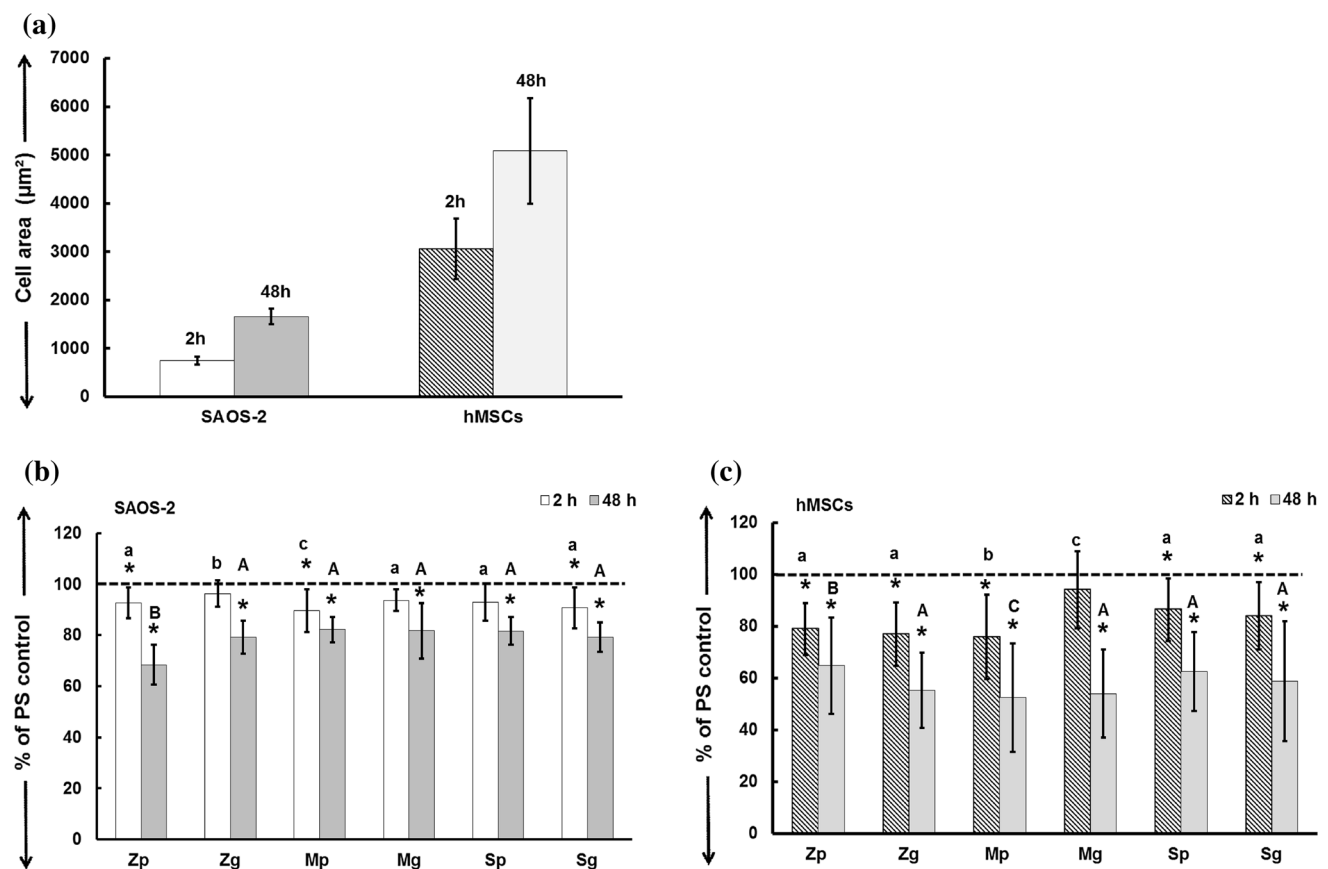

Fig. 6 Cell area after 2 and 48 h of cultivation on Ti samples. **a** Values of cell area on PS control in μm², **b** osteoblasts (SAOS-2)—relative values expressed as a percentage of PS control (*dashed line*), **c** human mesenchymal stem cells (hMSCs)—relative values expressed as a percentage of PS control (*dashed line*). *Asterisk* means a significant difference from PS control (Wilcoxon matched-pairs test, $p < 0.05$). Groups marked with *different lower-case letters* (2 h) or with *different upper-case letters* (48 h) express significant inter-group difference within samples (ANOVA, LSD post hoc test, $p < 0.05$)
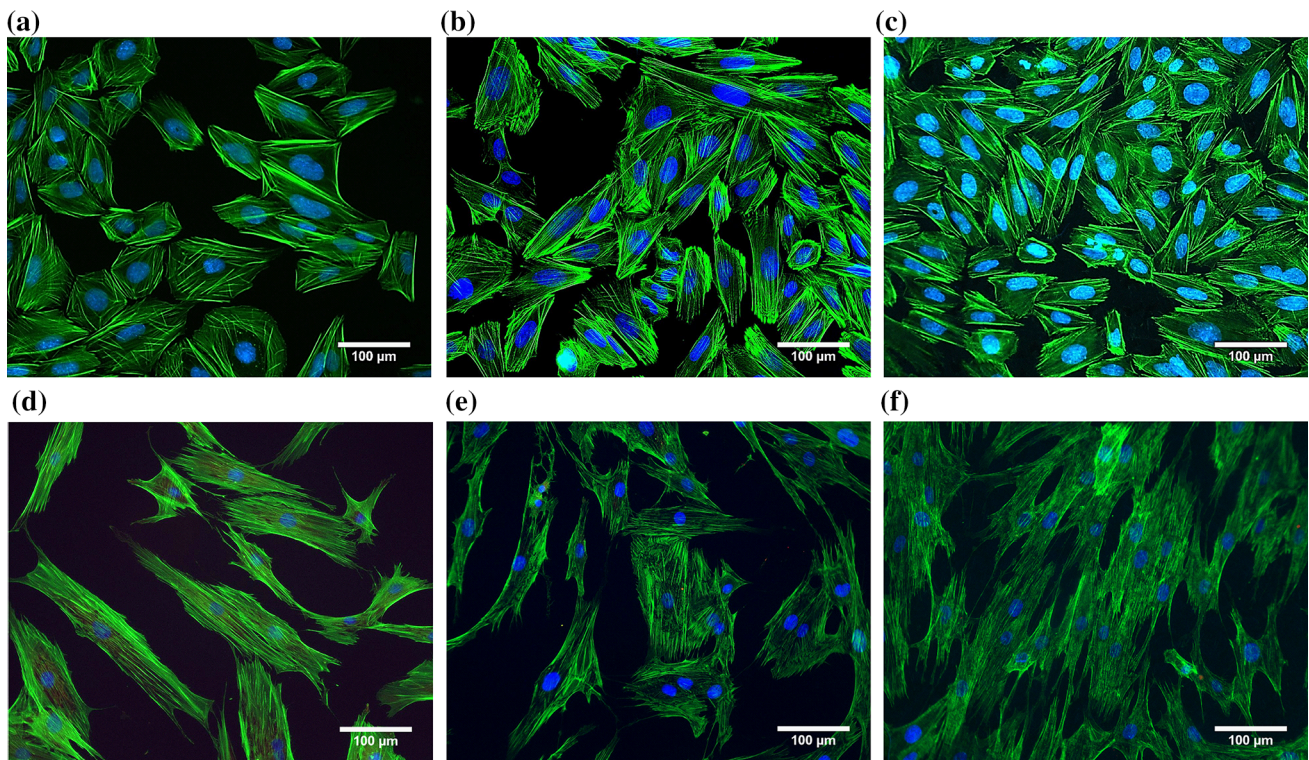
Fig. 7 Representative images of cells on different substrates after 48 h of cultivation. Osteoblasts (SAOS-2) (**a**–**c**) and human mesenchymal stem cells (hMSCs) (**d**–**f**) on PS control (**a**, **d**), polished sample (**b**, **e**), ground sample (**c**, **f**). Actin cytoskeleton stained by phalloidin-AF488 (*green*), nucleus stained by DAPI (*blue*)
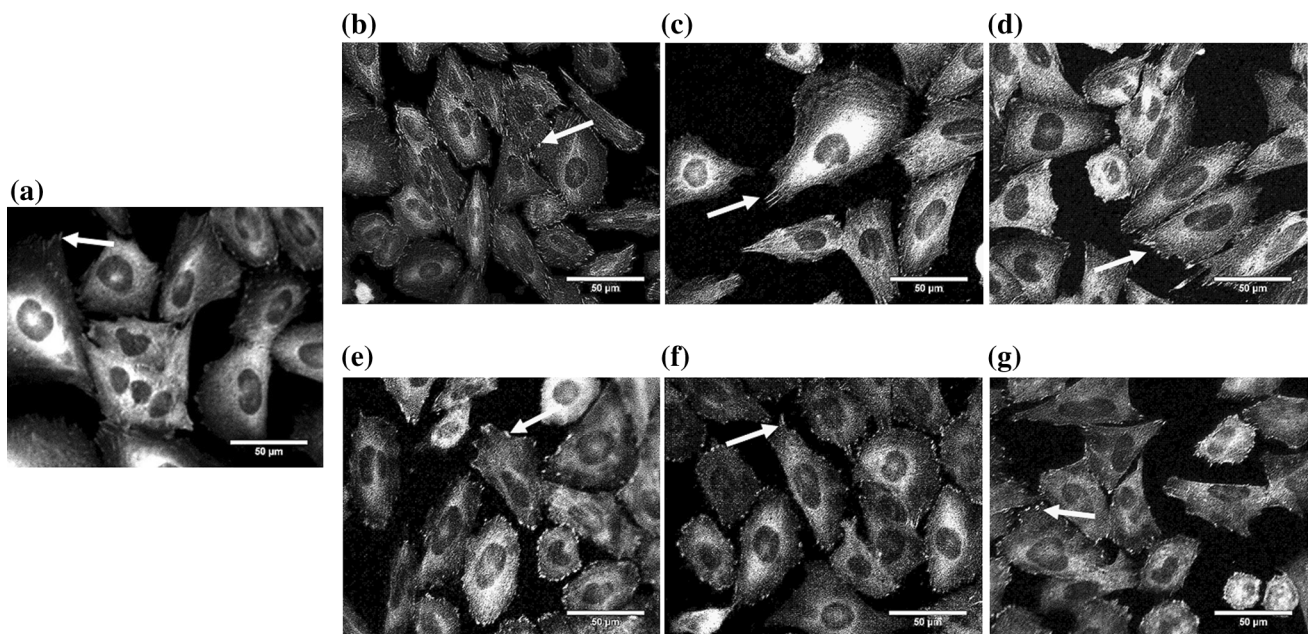

Fig. 8 Vinculin staining of osteoblasts (SAOS-2) on different substrates after 48 h of cultivation. **a** PS control, **b** Z polished sample, **c** M polished sample, **d** S polished sample, **e** Z ground sample, **f** M ground sample, **g** S ground sample. Vinculin as a protein of focal adhesion is stained by indirect immunofluorescent staining (secondary antibody conjugated with AF568). *Arrows* in the images point to the focal adhesion plaques

This study describes two novel UFG Ti materials with improved mechanical properties and different grain sizes produced by ECAP-Conform. This technique represents a repetitive modification of the standard ECAP, which can significantly reduce the costs of the previously expensive grain-refinement techniques and therefore enables a higher availability of UFG materials for biomedicine [27, 28]. The negligible number of impurities in our employed bulk cpTi Grade 2 (Table 1) is an important input parameter that is often difficult to achieve [29]. Recently, there have been a number of studies of materials that are distinguished for their immense mechanical strength during excessive stress [30, 31]. This report, however, focuses on the fact that implant materials must not only meet the criteria of sufficient tensile strength to fulfill their main purpose in tissue replacement, but they also must have an appropriate level of ductility. A balanced combination of these parameters was achieved in our tested UFG Ti (Fig. 1).

The influence of polishing and grinding on the surface topography of Ti samples characterized by AFM showed that polished samples differed despite the fact that the identical polishing method was used; therefore, grain size influenced the final surface topography after the samples were polished. For examples, AFM image of the sample Mp (Fig. 3) shows many spikes. The size of those spikes corresponds well to the size of Ti grains (4.6 μm) used for Mp sample preparation. Thus, those spikes can be the top parts of Ti grains drown into Ti sample, which were not removed during polishing. On the other hand, the surfaces of ground samples were most likely defined by the morphology of the abrasive paper and not by the grain size. The number of different topographical features (pits, peaks, tall objects) could have a strong influence on the adhesion, growth, and morphology of cultivated cells. High amounts of nano-scaled peaks are not recognized by the cells as a rough surface; thus, the cells tend to behave as if they are seeded on a completely flat surface. Moreover, these nano-sized objects appear to have no strong influence on cell behavior [32]. In contrast, many tall micro-scaled objects are considered unsuitable for cell growth because of a lack of places for proper cell attachment [32]. Generally, the combination of nano- and micro-scaled structures is currently considered the most suitable surface topography for supporting cell adhesion and growth [19, 33]. This statement was also approved for in vitro [34] and in vivo dental applications [35]. According to the literature, Ti samples represent usually the surfaces with contact angles around 70°–80° [18, 19, 33]. Significantly lower θ_A values (46°–49°) observed for the polished Ti samples in our study resulted from a proper removal of the oily impurities from the machine fabrication. The grinding process provided surfaces with the roughness R_{RMS} of two orders higher than that of the polished surfaces. The increasing surface roughness imprinted on further decrease in θ_A. This observation correlates with the literature where wettability increased with increasing roughness of hydrophilic surfaces [36]. This effect is explained by spreading the water drop through the rough features, thus decreasing the values of θ [37]. Additionally, Webb et al. [38] confirmed that the hydrophilic character of the materials increases the initial cell attachment and spreading compared to more hydrophobic materials. Although the polished samples were stated to be more hydrophobic compared with the ground samples, both samples had hydrophilic character, with θ values of approximately 40°, and should both be favorable for cell attachment.

Based on the cell metabolic activity results, a key observation is that none of the tested Ti samples had a significant negative effect on the metabolic activity of SAOS-2 cells and hMSCs after 48 h of cultivation. All the measured values of metabolic activity were higher than 75 % of the control, which is the value that determines cytotoxicity [39]. We determined that all manufactured types of Ti samples are non-cytotoxic and do not extensively harm the cells. Other authors have shown that more pronounced differences in osteoblast metabolic activity are noticeable after longer incubation times up to 7 days, when the hampered cell–cell communication on the rough surface may depress cell functions and the differences between cells cultivated on different materials may be more evident [40]. Comparing the results of cell number and metabolic activity, despite the high level of initial SAOS-2 cell attachment to the Ti samples, the further growth of cells was slowed. This statement is consistent with the findings of Kubo et al. [41], who found that the number of osteoblasts was dramatically higher on a rugged surface during the first hours of attachment, but that the proliferation rate on the rugged surfaces was lower compared to that on smooth surfaces after 24 h of incubation. Surprisingly, after 48 h of cultivation, the cell number of SAOS-2 on the Ti samples was higher than that on the PS control, but the metabolic activity remained similar on all the tested surfaces (Fig. 4a). This controversy could be explained by the adaptation of the cells to the surface of the Ti samples, accompanied by a slight reduction in metabolic activity during the 48 h of cultivation compared to the PS control, possibly indicating the initiation of the differentiation process, which appears earlier on osteoinductive materials such as Ti than on materials prepared only for optimal cell adhesion and growth [42]. Additionally, an MTS assay is often used as a tool for the assessment of the number of cells [40, 43]; however, we suggest that this assay is not suitable for the present study. To prevent the over- or underestimation of cell growth [44], the MTS assay should be accompanied by a method based on different principles (cell count, protein, or DNA quantification).

The decreased proliferation found in osteoblasts was found also in hMSCs. The decrease in hMSC proliferation could also be the consequence of their adaptation to the ultra-fine topography of the Ti sample surfaces within 48 h or of earlier initiation of differentiation induced by the material.

Although the results showed that the cells on the Ti samples were significantly smaller than those on the PS control, a visual inspection (Fig. 7) demonstrated that they spread on all tested surfaces, evenly forming high-density clusters. However, notably, the hMSCs were isolated from different donors; thus, the results of each measurement were highly dependent on the state of the donor at the time of the biopsy. The possible influence of the material on the size of the cells was also observed by Zinger et al. [45], who found a correlation between rough surface topography and decreased cell area. These authors hypothesized that the rougher the surface, the thicker the cells are as they spread more into the structures and minimally into the horizontal line.

The influence of the material surface topography on the cell morphology and spreading was previously described and confirmed [20, 32, 33]. In our study, we observed that the polished surfaces with nano-topography approaching a flat surface did not force the cells to spread and elongate to find better places to fit. In contrast, the cells cultivated on the rough ground surfaces with a combination of nano- and microstructures were usually elongated or had a greater number of variable shapes as they attempted to cope with the rugged substrate (Fig. 8e–g). The findings of focal adhesions suggest that SAOS-2 cells cultured on the rough surface of the ground samples tend to form focal adhesions on their extensions while they grow and mimic the surface. Smooth topography does not force the cells to exhibit large focal adhesions, and SAOS-2 cells are anchored around their bottom poles (Fig. 8b–d). The same statement was also confirmed for hMSCs. However, their vinculin signal was hardly detectable; thus, the data are not shown.

Taken together, our study highlighted the possibility of a cost-saving fabrication of the mechanically advanced Ti material (Z sample), while maintaining the excellent biological properties of the original Ti (S sample), and the usage of this material in dental implant applications.

Conclusion

The aim of this work was to evaluate the short-time biological responses of human osteoblasts and mesenchymal stem cells to the newly developed ultra-fine grain Ti materials with enhanced mechanical resistance and long-term performance. Two novel types of the original Ti were produced, and the surfaces of all tested Ti samples were subsequently treated by polishing or grinding. The samples differed in grain size, final surface topography, and wettability, where the rough ground samples showed increased hydrophilicity compared to the polished samples, irrespective of the grain size. Both cell types attached onto all Ti samples in a significantly higher amount than onto the PS control. Additionally, the cytocompatibility of the Ti samples was evaluated by metabolic activity, and the favorable spreading of osteoblasts confirmed that all the Ti samples had exceptional properties suitable for osteoblast growth and future bone implant development. Although the hMSCs displayed lower cell numbers and metabolic activity compared to osteoblasts, the Ti samples were shown to be suitable surfaces for their growth and possible osteoblast-like differentiation.

The increased strength and longevity of commercially pure Grade 2 Ti are highly demanded dental implant material properties, and the construction of reliable implants remains a topic of discussion. This new ultra-fine grain Ti can successfully compete with the present materials utilized in dentistry due to its balanced mechanical properties which provide high toughness in the stress conditions in the oral cavity while keeping its formability for further processing of various implants. Moreover, its considerably lower production costs and excellent biocompatibility make this Ti an affordable material for subsequent utilization in the development of dental implants.

References

1. Cordova LA, Stresing V, Gobin B, Rosset P, Passuti N, Gouin F et al (2014) Orthopaedic implant failure: aseptic implant loosening—the contribution and future challenges of mouse models in translational research. Clin Sci (Lond) 127:277–293

2. Chrcanovic BR, Albrektsson T, Wennerberg A (2014) Immediate nonfunctional versus immediate functional loading and dental implant failure rates: a systematic review and meta-analysis. J Dent 42:1052–1059

3. Ren K, Dusad A, Zhang Y, Purdue PE, Fehringer EV, Garvin KL et al (2014) Early diagnosis of orthopedic implant failure using macromolecular imaging agents. Pharm Res 31:2086–2094

4. Gawkrodger DJ (2003) Metal sensitivities and orthopaedic implants revisited: the potential for metal allergy with the new metal-on-metal joint prostheses. Br J Dermatol 148:1089–1093

5. Plecko M, Sievert C, Andermatt D, Frigg R, Kronen P, Klein K et al (2012) Osseointegration and biocompatibility of different

metal implants–a comparative experimental investigation in sheep. BMC Musculoskelet Disord 13:32

6. Browne M, Gregson PJ (2000) Effect of mechanical surface pretreatment on metal ion release. Biomaterials 21:385–392

7. Mishnaevsky L, Levashov E, Valiev RZ, Segurado J, Sabirov I, Enikeev N et al (2014) Nanostructured titanium-based materials for medical implants: modeling and development. Mater Sci Eng R 81:1–19

8. Greger M, Cerny M, Kander L, Kliber J (2009) Structure and properties of titanium for dental implants. Metalurgija 48:249–252

9. Niinomi M (2002) Recent metallic materials for biomedical applications. Metall Mater Trans A 33:477–486

10. Hallab NJ, Anderson S, Caicedo M, Brasher A, Mikecz K, Jacobs JJ (2005) Effects of soluble metals on human peri-implant cells. J Biomed Mater Res Part A 74:124–140

11. Greger M, Kander L, Masek V, Vlcek M (2010) Ultra fine grain titanium using for medical applications—structure and properties. In: Nanocon 2010, 2nd international conference, pp 502–507

12. Yu ZT, Zhang MH, Tian YX, Cheng J, Ma XQ, Liu HY et al (2014) Designation and development of biomedical Ti alloys with finer biomechanical compatibility in long-term surgical implants. Front Mater Sci 8:219–229

13. Schram SE, Warshaw EM, Laumann A (2010) Nickel hypersensitivity: a clinical review and call to action. Int J Dermatol 49:115–125

14. Valiev RZ, Estrin Y, Horita Z, Langdon TG, Zehetbauer MJ, Zhu YT (2006) Producing bulk ultrafine-grained materials by severe plastic deformation. JOM 58:33–39

15. Valiev RZ, Langdon TG (2006) Principles of equal-channel angular pressing as a processing tool for grain refinement. Prog Mater Sci 51:881–981

16. Kubina T, Dlouhy J, Kover M, Domankova M, Hodek J (2015) Preparation and thermal stability of ultra-fine and nano-grained commercially pure titanium wires using conform equipment. Mater Tehnol 49:213–217

17. Kubina T, Dlouhy J, Kover M, Hodek J (2014) Study of thermal stability of ultra fine-grained commercially pure titanium wire prepared in conform equipment. Metallography Xv 782:415–420

18. Estrin Y, Ivanova EP, Michalska A, Truong VK, Lapovok R, Boyd R (2011) Accelerated stem cell attachment to ultrafine grained titanium. Acta Biomater 7:900–906

19. Gittens RA, McLachlan T, Olivares-Navarrete R, Cai Y, Berner S, Tannenbaum R et al (2011) The effects of combined micron-/submicron-scale surface roughness and nanoscale features on cell proliferation and differentiation. Biomaterials 32:3395–3403

20. Teng FY, Ko CL, Kuo HN, Hu JJ, Lin JH, Lou CW et al (2012) A comparison of epithelial cells, fibroblasts, and osteoblasts in dental implant titanium topographies. Bioinorg Chem Appl 2012:687–792

21. Le Guehennec L, Soueidan A, Layrolle P, Amouriq Y (2007) Surface treatments of titanium dental implants for rapid osseointegration. Dent Mater 23:844–854

22. Weber HP, Cochran DL (1998) The soft tissue response to osseointegrated dental implants. J Prosthet Dent 79:79–89

23. Rezek B, Ukraintsev E, Kratka M, Taylor A, Fendrych F, Mandys V (2014) Epithelial cell morphology and adhesion on diamond films deposited and chemically modified by plasma processes. Biointerphases 9:031012

24. Pop-Georgievski O, Kubies D, Zemek J, Neykova N, Demianchuk R, Mazl Chanova E et al (2015) Self-assembled anchor layers/polysaccharide coatings on titanium surfaces: a study of functionalization and stability. Beilstein J Nanotechnol 6:617–631

25. Schneider CA, Rasband WS, Eliceiri KW (2012) NIH Image to ImageJ: 25 years of image analysis. Nat Methods 9:671–675

26. Carpenter AE, Jones TR, Lamprecht MR, Clarke C, Kang IH, Friman O et al (2006) Cell Profiler: image analysis software for identifying and quantifying cell phenotypes. Genome Biol 7:R100

27. Dyakonov GS, Gu CF, Toth LS, Valiev RZ, Semenova IP (2014) Microstructure and mechanical properties of continuous equal channel angular pressed titanium. In: 6th international conference on nanomaterials by severe plastic deformation (Nanospd6), vol. 63

28. Polyakov AV, Semenova IP, Valiev RZ (2014) High fatigue strength and enhanced biocompatibility of UFG CP Ti for medical innovative applications. In: 6th international conference on nanomaterials by severe plastic deformation (Nanospd6), vol. 63

29. Li HL, Oppenheimer SM, Stupp SI, Dunand DC, Brinson LC (2004) Effects of pore morphology and bone ingrowth on mechanical properties of microporous titanium as an orthopaedic implant material. Mater Trans 45:1124–1131

30. Mall S, Cunningham SR (2007) Fatigue behavior of integrally fabricated joints between titanium matrix composite and titanium alloy. Compos Struct 80:65–72

31. Zhao XC, Fu WJ, Yang XR, Langdon TG (2008) Microstructure and properties of pure titanium processed by equal-channel angular pressing at room temperature. Scr Mater 59:542–545

32. Broz A, Baresova V, Kromka A, Rezek B, Kalbacova M (2009) Strong influence of hierarchically structured diamond nanotopography on adhesion of human osteoblasts and mesenchymal cells. Phys Status Solidi A 206:2038–2041

33. Chen XY, Cai KY, Lai M, Zhao L, Tang LL (2012) Mesenchymal stem cells differentiation on hierarchically micro/nanostructured titanium substrates. Adv Eng Mater 14:B216–B223

34. Naddeo P, Laino L, La Noce M, Piattelli A, De Rosa A, Iezzi G et al (2015) Surface biocompatibility of differently textured titanium implants with mesenchymal stem cells. Dent Mater 31:235–243

35. Elias CN, Fernandes DJ, Resende CRS, Roestel J (2015) Mechanical properties, surface morphology and stability of a modified commercially pure high strength titanium alloy for dental implants. Dent Mater 31:E1–E13

36. Garbassi F, Mora M, Ochiello E (1994) Polymer surfaces: from physics to technology, 1st edn. Wiley, New York

37. Ponsonnet L, Reybier K, Jaffrezic N, Comte V, Lagneau C, Lissac M et al (2003) Relationship between surface properties (roughness, wettability) of titanium and titanium alloys and cell behaviour. Mater Sci Eng C 23:551–560

38. Webb K, Hlady V, Tresco PA (1998) Relative importance of surface wettability and charged functional groups on NIH 3T3 fibroblast attachment, spreading, and cytoskeletal organization. J Biomed Mater Res 41:422–430

39. Flahaut E, Durrieu MC, Remy-Zolghadri M, Bareille R, Baquey C (2006) Investigation of the cytotoxicity of CCVD carbon nanotubes towards human umbilical vein endothelial cells. Carbon 44:1093–1099

40. Zhao LZ, Mei SL, Chu PK, Zhang YM, Wu ZF (2010) The influence of hierarchical hybrid micro/nano-textured titanium surface with titania nanotubes on osteoblast functions. Biomaterials 31:5072–5082

41. Kubo K, Tsukimura N, Iwasa F, Ueno T, Saruwatari L, Aita H et al (2009) Cellular behavior on TiO_2 nanonodular structures in a micro-to-nanoscale hierarchy model. Biomaterials 30:5319–5329

42. Klein MO, Bijelic A, Toyoshima T, Gotz H, von Koppenfels RL, Al-Nawas B et al (2010) Long-term response of osteogenic cells on micron and submicron-scale-structured hydrophilic titanium surfaces: sequence of cell proliferation and cell differentiation. Clin Oral Implant Res 21:642–649

43. Guida L, Oliva A, Basile MA, Giordano M, Nastri L, Annunziata M (2013) Human gingival fibroblast functions are stimulated by oxidized nano-structured titanium surfaces. J Dent 41:900–907

44. Maghni K, Nicolescu OM, Martin JG (1999) Suitability of cell metabolic colorimetric assays for assessment of CD4+ T cell proliferation: comparison to 5-bromo-2-deoxyuridine (BrdU) ELISA. J Immunol Methods 223:185–194

45. Zinger O, Anselme K, Denzer A, Habersetzer P, Wieland M, Jeanfils J et al (2004) Time-dependent morphology and adhesion of osteoblastic cells on titanium model surfaces featuring scale-resolved topography. Biomaterials 25:2695–2711